Schweizerische Eidgenossenschaft
Confédération suisse
Confederazione Svizzera
Confederaziun svizra

National Centre for Climate Services NCCS

CH2018

Klimaszenarien für die Schweiz

Schweizerische Eidgenossenschaft
Confédération suisse
Confederazione Svizzera
Confederaziun svizra

Eidgenössisches Departement des Innern EDI
Bundesamt für Meteorologie und Klimatologie MeteoSchweiz

MeteoSchweiz

ETH zürich

C2SM Center for Climate Systems Modeling

UNIVERSITÄT BERN

sc | nat

Science and Policy
Platform of the Swiss Academy of Sciences

ProClim
Forum for Climate and Global Change

Haupt-Projektpartner
Bundesamt für Meteorologie und Klimatologie MeteoSchweiz, ETH Zürich, Center for Climate Systems Modeling (C2SM)

Co-Projektpartner
Universität Bern, ProClim | SCNAT

Projektsteuerung
Mischa Croci-Maspoli (MeteoSchweiz), Reto Knutti (ETH Zürich), Mark A. Liniger (bis März 2017, MeteoSchweiz), Christoph Schär (ETH Zürich), Cornelia Schwierz (MeteoSchweiz)

Projektleitung
Andreas M. Fischer (MeteoSchweiz), Kuno M. Strassmann (C2SM, ETH Zürich)

Autoren des Technischen Grundlagenberichts (in alphabetischer Reihenfolge)
Nikolina Ban (ETH Zürich), Mathias Bavay (SLF), David N. Bresch (ETH Zürich, MeteoSchweiz), Stefan Brönnimann (Uni Bern), Paolo Burlando (ETH Zürich), Ana Casanueva (MeteoSchweiz), Mischa Croci-Maspoli (MeteoSchweiz), Fabienne Dahinden (ETH Zürich), Simone Fatichi (ETH Zürich), Iris Feigenwinter (MeteoSchweiz), Andreas M. Fischer (MeteoSchweiz), Erich M. Fischer (ETH Zürich), Sophie Fukutome (MeteoSchweiz), Michael Graf (Uni Bern), Martin Hirschi (ETH Zürich), Reto Knutti (ETH Zürich), Sven Kotlarski (Meteo-Schweiz), Hans-Ruedi Künsch (ETH Zürich), Mark A. Liniger (MeteoSchweiz), Olivia Martius (Uni Bern), Christoph Marty (SLF), Iselin Medhaug (ETH Zürich), Nadav Peleg (ETH Zürich), Moritz Pickl (MeteoSchweiz), Christoph C. Raible (Uni Bern), Jan Rajczak (ETH Zürich), Ole Rössler (Uni Bern), Christoph Schär (ETH Zürich), Simon C. Scherrer (MeteoSchweiz), Christina Schnadt Poberaj (C2SM, ETH Zürich), Cornelia Schwierz (MeteoSchweiz), Sonia I. Seneviratne (ETH Zürich), Maurice Skelton (ETH Zürich), Silje Sørland (ETH Zürich), Curdin Spirig (C2SM, ETH Zürich), Kuno M. Strassmann (C2SM, ETH Zürich), Mathias Trachsel (Uni Bern), Richard Wartenburger (ETH Zürich), Elias M. Zubler (MeteoSchweiz)

Begleitgruppe
Dörte Aller (PLANAT/SIA), Pierluigi Calanca (Agroscope), Arthur Gessler (WSL), Roland Hohmann (BAFU), Ole Rössler (Uni Bern), Damiano Urbinello (BAG)

Kommunikative Begleitung
Nina Aemisegger (MeteoSchweiz), Monika Gut (MeteoSchweiz), Michael Keller (ETH Zürich), Michael Walther (ETH Zürich)

Dank
Wir danken den 22 externen nationalen und internationalen Gutachterinnen und Gutachtern des Technischen Berichts für deren wertvolle Kommentare.

Konzeption dieser Broschüre
Kuno M. Strassmann (C2SM, ETH Zürich)

Redaktion
Andreas M. Fischer (MeteoSchweiz), Kuno M. Strassmann (C2SM, ETH Zürich)

Gestaltung & Infografik
Roland Ryser / zeichenfabrik.ch

Text
Sinnform AG

Herausgeber
National Centre for Climate Services NCCS
c/o Bundesamt für Meteorologie und Klimatologie MeteoSchweiz
Operation Center 1, Postfach 257
CH-8058 Zürich-Flughafen
www.nccs.ch

Zitierung
NCCS (Hrsg.) 2018: CH2018 - Klimaszenarien für die Schweiz. National Centre for Climate Services, Zürich. 24 S.
ISBN-Nummer 978-3-9525031-0-2

Bezug der gedruckten Fassung und PDF-Download
BBL, Verkauf Bundespublikationen, CH-3003 Bern
www.bundespublikationen.admin.ch
Art.-Nr.: 313.006.d
11.18 3500 860430189

Klimaneutral und VOC-arm gedruckt auf Recyclingpapier
Diese Publikation ist auch in französischer, italienischer und englischer Sprache verfügbar.

gedruckt in der schweiz

Klimaneutral
Druckprodukt
ClimatePartner.com/53460-1810-1002

3. Reference climate and recent change

Summary

Switzerland is situated in the zone of the westerlies in the northern mid-latitudes. Cyclones and fronts bring moist air from the nearby Atlantic Ocean and seas to Switzerland, intermitted by phases of high pressure with stable weather. The complex topography of the Alps creates a diverse climate with large altitudinal and spatial gradients and small-scale phenomena. Detailed information on the country's past and present climate is presented for temperature, heat stress, precipitation, snow, and wind.

Long-term high-quality measurements of the climate exist for the last 150 years, and reconstructions for some variables are available for the last 330 years. Despite large natural variability on timescales of years to decades, a robust climate-change signal is found for several variables.

- Near-surface air temperature has increased by about 2.0 °C between 1864 and 2017, compared to 0.9 °C globally, with most of the warming taking place since the 1980s. The 1988 to 2017 summer average is by far the warmest 30-year summer average since the start of reliable reconstructions in 1685. This warming has led to more frequent and more intense heat waves; meanwhile, cold periods have become less frequent. The zero-degree line has risen by 300 m to 400 m since the 1960s.
- The temperature increase has had pronounced effects on the cryo- and biosphere. The volume of Alpine glaciers has decreased by about 60 % since the 1850s. Since the 1970s, the number of snow days and snowfall days has decreased by about 20 % at about 2000 m a.s.l. to 50 % below 800 m a.s.l. The vegetation period and pollen season are two to four weeks longer today than in the 1960s.
- Winter precipitation has increased by about 20 % to 30 % since 1864, although part of this apparent change may be due to natural variability. There are robust signals that heavy precipitation has become more frequent (+30 %) and more intense (+12 %) since the beginning of the 20th century.
- Sunshine duration, a proxy for global radiation, shows a significant decline of -15 % between the 1950s and around 1980, followed by a significant increase of +20 % to the present day.

No robust signals on long-term trends in the observational record are found for summer precipitation, droughts, wind speed, or low stratus. For these quantities, it is either unclear at this point how they are affected by climate change, or the expected anthropogenic signal has not yet emerged from the observed large natural variability (e.g., summer drying). The observational basis is too short or insufficient to make robust inferences about past changes in small-scale phenomena such as thunderstorms, tornadoes, and hail.

Comprehensive knowledge of the past and present-day climate and its variability is indispensable in the process of securing a reference for potential future climate change, validating and correcting climate models, and assessing the significance of the observed and projected trends. A comparison of observed and modeled trends in the past is essential in efforts to reveal the driving physical processes. In addition, high-quality long-term observational datasets are key for the estimation of the range of variability intrinsic to the climate system. This further allows estimation of natural variability and assessment of the significance of the projected changes.

In this chapter, the large-scale setting and relevant drivers of the Swiss climate are introduced first (Chapter 3.1). The main features and the mean state – setting the reference for the projected changes – are then described in Chapter 3.2. Finally, the observed variability and recent changes are presented in Chapter 3.3, using observations and some reconstructions from climate proxies.

3.1. Drivers of the Swiss climate

3.1.1. Introduction

The general characteristics of the Swiss climate are mainly determined by Switzerland's geographical position and the corresponding dynamical processes dominant in this climate zone. The local characteristics can be strongly modified by the complex topography of the Alps. In this section, the focus is on the large-scale setting and variability, the effects of the Alps, and local feedbacks.

3.1.2. Large-scale setting and variability

Switzerland and the Alps are situated in the northern mid-latitudes and the so-called "temperate climate zone" [221]. The synoptic-scale flow is strongly determined by the eastward passage of fronts, cyclones, and anticyclones determining the day-to-day weather variation, albeit with pronounced seasonal differences (e.g., [5]). In winter (DJF), large pressure gradients and considerable variability in the pressure field are caused by low- and high-pressure systems and fronts impinging upon the Alpine region (Figure 3.1). The latter effect is illustrated by the percentage share of the ten "Grosswettertypen" based on the geopotential height at 500 hPa (GWT10 Z500) [263, 229], which indicates that the flow for both summer and winter is dominated by advection from the west, northwest, and southwest, as well as from the north.

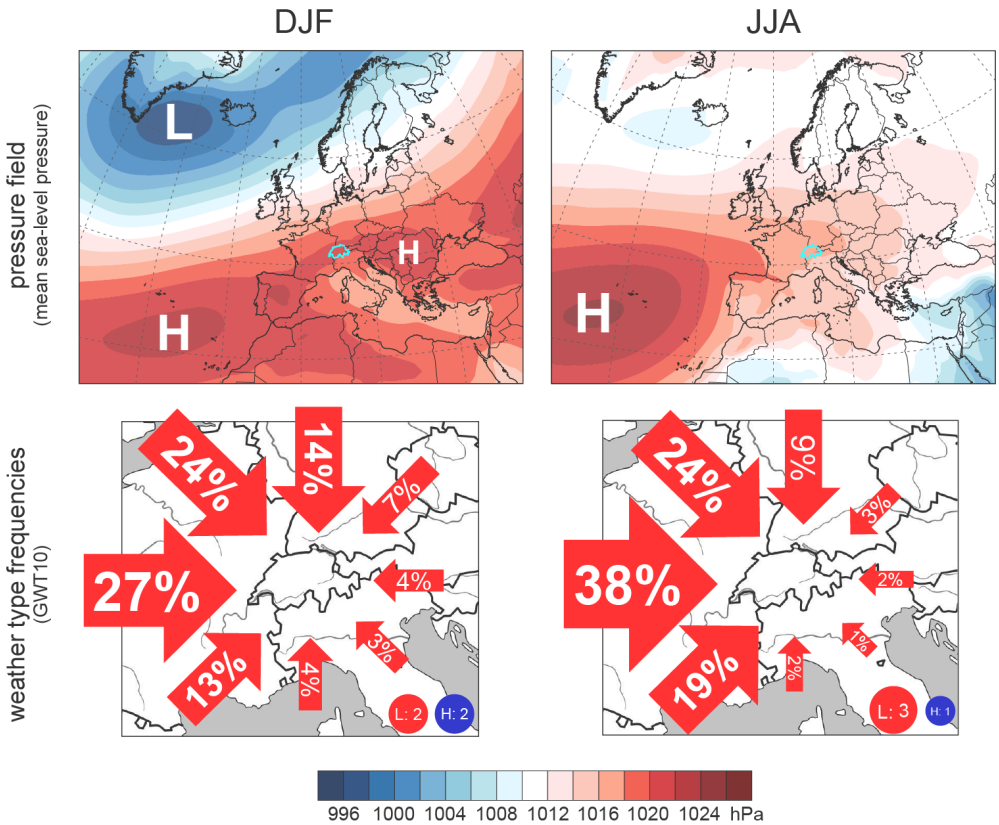

Figure 3.1. Seasonal mean sea-level pressure (hPa) over Europe (top) and the portion of incident flow (bottom) expressed as the percentage share of the ten GWT10 Z500 weather types over Switzerland for winter (left, December to February) and summer (right, June to August). The GWT10 Z500 types represent flow from the N: north, NE: north-east, E: east, SE: south-east, S: south, SW: southwest, W: west, NW: northwest, and L: low pressure, H: high pressure. The period considered is 1981 - 2010. The Swiss borders are shown in light blue in the top panels.

The day-to-day variability of sea-level pressure is large, and the distribution is negatively skewed (long left tail) in winter (standard deviation ~10 hPa, Figure 3.2). The small values are caused by low-pressure systems impinging upon the Alps. In summer, the variability is much smaller (~4 hPa), and the distribution is highly symmetrical (Figure 3.2). In summary, the difference between the winter and summer pressure distributions nicely illustrates the strong seasonality typical of a mid-latitude climate.

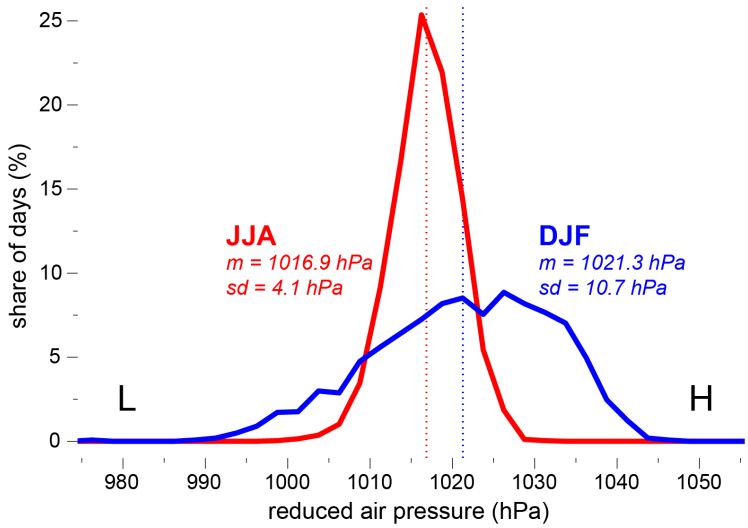

Figure 3.2. Distributions of the daily reduced sea-level air pressure at the Zurich/Fluntern station for winter (December to February, blue) and summer (June to August, red). The mean pressure (m, dotted vertical lines and numbers) is higher and the pressure is much more variable (standard deviation sd, numbers) in winter compared to summer. The values have been binned into 2.5 hPa bins to compute the share of days per bin. L stands for "low pressure", H for "high pressure".

On the monthly and seasonal scale, the effect of weather systems is usually expressed by the dominant modes of flow variability using pressure fields (e.g., [364, 14]). The most prominent mode in the Euro-Atlantic region is the North Atlantic Oscillation (NAO), which explains about one-third of the variance in sea-level pressure in winter [363, 161, 368] and also substantial fractions of temperature and precipitation variability. Other common modes explaining considerable amounts of temperature and precipitation variability (e.g., [51]) are the East Atlantic (EA) pattern, the East Atlantic/Western Russia (EAWR) pattern (sometimes also called the Eurasia-2 pattern), and the Scandinavian (SCAN) pattern (also called the Eurasia-1 pattern) [14].

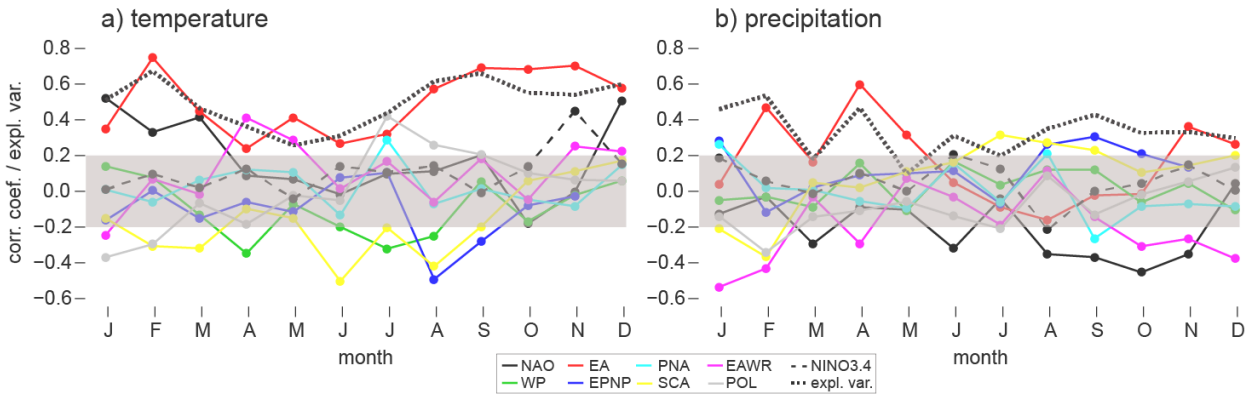

Figure 3.3. Influence of the eight major modes of climate variability of the Northern Hemisphere and the El Niño Southern Oscillation (ENSO, shown as NINO3.4 index) on Swiss temperature and precipitation variability for the time period 1950 - 2017. Shown is the Pearson correlation of the corresponding mode with northern Swiss temperature (a) and precipitation (b). The dashed bold black lines indicate the fraction of the variance explained by a stepwise linear regression model using the eight major climate modes of the Northern Hemisphere plus ENSO as the explaining time series. The grey band shows the range of insignificant correlations (p=0.05). The monthly climate mode indices used here are produced by the Climate Prediction Center of NCEP/NOAA (ftp.cpc.ncep.noaa.gov/wd52dg/data/indices/). NAO: North Atlantic Oscillation, EA: East Atlantic Pattern, PNA: Pacific/North American pattern, EAWR: East Atlantic/West Russia pattern, WP: West Pacific pattern, EPNP: East Pacific/North Pacific pattern, SCA: Scandinavian pattern, POL: Polar/Eurasia pattern.

Figure 3.3 gives an overview of the influence of the major modes of climate variability on Swiss temperature and precipitation variability. The EA-like pattern (red line) has a substantially larger influence on the interannual Swiss temperature variability than the NAO (black line; cf. [294]). The influence of the NAO is somewhat more pronounced at higher altitudes and in southern Switzerland, especially in winter (not shown). For winter and spring precipitation, the blocking-like EAWR (purple line) and EA (red line) patterns explain substantial fractions of interannual variability. The eight major climate modes of the

Northern Hemisphere explain about 50 - 70 % of interannual Swiss winter temperature variability and 30 - 55 % of interannual Swiss winter precipitation variability (dashed red lines in Figure 3.3). The direct influence of the most dominant global climate mode, the El Niño Southern Oscillation (ENSO, shown as Nino3.4 index, dashed black line), on Switzerland is generally small. Some studies have hypothesized a more significant impact of the ENSO on Europe in the past (e.g., [119, 43]).

In summer (JJA), the pressure gradients are much smaller than in winter, and the Azores high is the dominant large-scale pressure system, leading to reduced variability over Switzerland (cf. Figure 3.1). The flow is still dominated by advection from westerly directions and from the north, but the influence of modes of flow variability is reduced. Consequently, local processes and feedbacks become important, as the following section explains.

3.1.3. Effects of the Alps

The Alps with their complex topography considerably influence the Swiss weather and climate (see [304] for an overview). The synoptic systems impinging upon the Alps are strongly modified, leading to effects often associated with severe weather such as frontal bending and lee cyclogenesis south of the Alps. Regional wind systems and gravity waves are triggered. The two most well-known regional wind systems are the Föhn (e.g., [329]), which is a flow crossing the main ridge, and the Bise [366], an example of deflected flow. Other examples of deflected flow in the greater Alpine region are the Mistral [259] and the Bora [327, 137]. Several smaller-scale features such as thermally driven circulation (mountain-valley flow; e.g., [247]), lee waves, and deep convective clouds are also common.

The interplay between the flow and the complex topography leads to spatially highly variable meteorological fields. This is especially the case for precipitation, where factors such as orographic enhancement, rain shadow effects, and enhanced convective activity modify the precipitation field. Due to low temperatures, a substantial amount of precipitation falls as snow, especially at higher altitudes that feature glaciers and permafrost (e.g., [160]). Favored by cold-air pooling, fog and low stratus are often found in the pre-Alpine basins in the winter half year.

3.1.4. Local feedback processes

Especially in summer, when large-scale pressure gradients are small (cf. Figure 3.1), local feedbacks can generate small-scale climate variability and extreme weather events. An important feedback in this respect is the soil moisture-temperature feedback. This is known to be a strong driver of temperature extremes in many regions across the globe with a transition climate (i.e., between humid and arid) and could strongly affect future temperature extremes in Europe and Switzerland as well (cf. [313, 111, 315, 156, 239] and Chapter 6.7 for more details). Another feedback coming into play in spring and summer, especially at higher altitudes, is the snow-albedo feedback, which can modify spring temperatures at the snowline by a few tenths of a degree [293, 384].

3.2. Reference climate

This section introduces the Swiss reference climate, which has already been influenced by climate change. The climate-change signal is discussed in detail in Chapter 3.3. The reference climate is the same as or as similar as possible to the mean reference state of the CH2018 scenarios (the 30-year reference period 1981 - 2010; cf. Chapter 2.3). The variables of near-surface (2-meter) temperature, mean, heavy, and extreme precipitation, snowpack, and wind are considered in detail. For other variables, additional resources are provided. The observational network density available is different for each variable, but is generally very dense compared to most other mountainous regions in the world (cf. Chapter 2.6).

3.2.1. Temperature and heat stress

Switzerland spans an altitude range from 193 m a.s.l. to 4634 m a.s.l. Accordingly, the temperature range in Switzerland is large. The lowest temperature officially measured by MeteoSwiss in Switzerland was -42.5 °C in La Brévine (1048 m a.s.l.) on January 12, 1987; the highest temperature was +41.5 °C in Grono (382 m asl)

on August 11, 2003 (source: MeteoSwiss). Most regions on the Swiss Plateau have experienced absolute minima between -20 °C and -25 °C and absolute maxima between +35 °C and +40 °C in the reference period. Temperatures above 40 °C have only been recorded once in Switzerland thus far.

Figure 3.4 shows normal values (averages over the reference period) for the monthly mean of daily maximum, mean, and minimum temperature at four Swiss meteorological stations situated in four different climatic zones (southern Swiss lowlands at ~300 m a.s.l., Swiss Plateau at ~550 m a.s.l., eastern Swiss Alps at ~1600 m a.s.l., and central Alps at almost 3600 m a.s.l.). The temperature has a strong seasonal cycle, with minima in January or February and maxima in July. The seasonal cycle is somewhat less pronounced at the high-altitude stations than at the low-altitude stations. At higher altitudes (> ~2000 m a.s.l.), the monthly mean temperature minima (TN) are below 0 °C during most of the year. At very high altitudes (> 3500 m a.s.l.), the monthly mean temperature maxima (TX) rises above 0 °C only in the summer months (cf. Figure 3.5, bottom left). At low altitudes, in contrast, monthly mean temperatures ™ are close to 0 °C only in the coldest winter months (cf. Figure 3.5, top center), whereas in summer, monthly mean temperature maxima (TX) can reach almost 25 °C in northern Switzerland and even higher in southern Switzerland (Figure 3.5, bottom left).

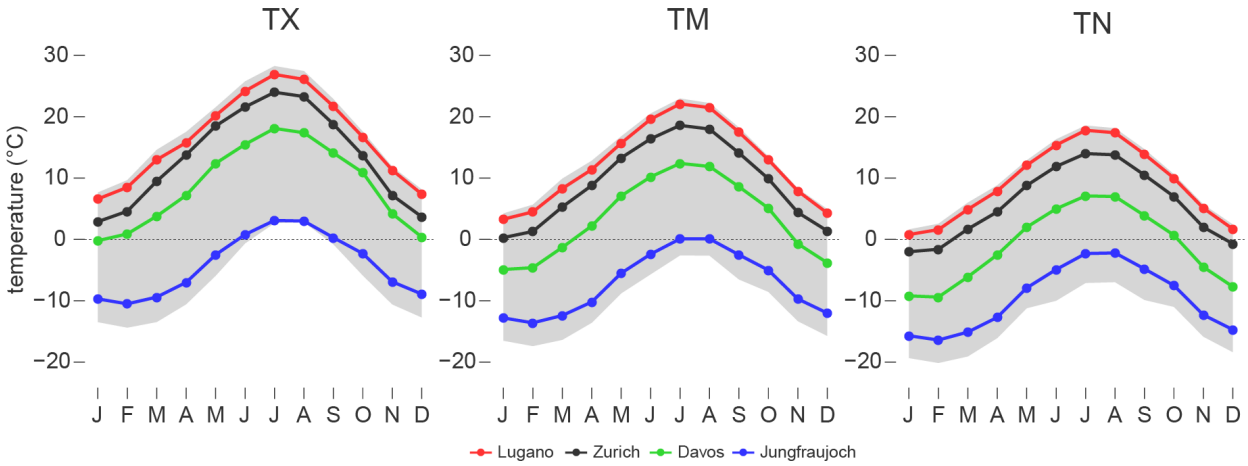

Figure 3.4. Monthly normal values (mean of period 1981 - 2010) for daily maximum (TX, left), mean (TM, center), and minimum (TN, right) temperature in °C at four Swiss stations: Lugano (red, 273 m a.s.l.), Zürich/Fluntern (black, 556 m a.s.l.), Davos (green, highest city in the Swiss Alps at 1594 m a.s.l.), and Jungfraujoch (blue, high mountain station at 3580 m a.s.l.). The grey band shows the range of all values in Switzerland using the MeteoSwiss gridded temperature products [123].

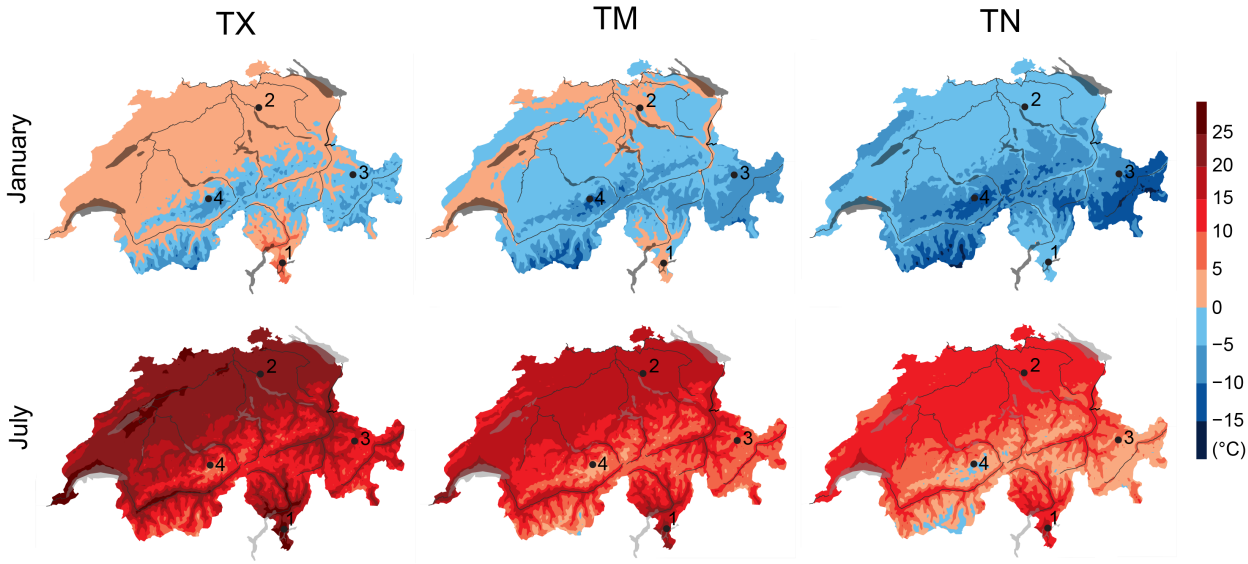

Figure 3.5. Maps of monthly normal values (mean of period 1981 - 2010) for maximum (TX, left column), mean (TM, middle column), and minimum (TN, right column) temperature in °C for January (top row) and July (bottom row). The dots and numbers show the locations of the four stations used in Figure 3.4: 1: Lugano, 2: Zürich/Fluntern, 3: Davos, and 4: Jungfraujoch. Data: MeteoSwiss gridded temperature products [123].

Very high temperatures during the night and day greatly affect human health and well-being. Heat exposure can raise the core body temperature and thus cause heat-related illnesses and impact productivity [188]. The effect of temperature on the human body is enhanced by the relative humidity. When the external temperature is high, the only way for the body to stay at a healthy temperature is through loss of heat via sweat evaporation. However, high external air humidity and certain clothing (e.g., protective clothing worn in certain jobs) limit sweat evaporation, forcing core body temperature to rise [348]. Under such circumstances, the combination of external heat exposure and internal heat production generated from metabolic processes can provoke heat stress [386]. There are many heat stress indices in the literature that attempt to quantify heat stress in a single value (see [28, 63] for a review). In this report, the Wet Bulb Temperature (TW) has been selected to describe heat stress conditions [321, 74, 253]. TW is the temperature an air parcel would attain if cooled at constant pressure until saturation by the evaporation of water into it; it equals the air (dry bulb) temperature when relative humidity is 100 %. TW can be measured by covering a standard thermometer bulb with a wet cloth and fully ventilating it. In contrast to more sophisticated heat stress indices, such as the Wet Bulb Globe Temperature [204] or the Universal Thermal Climate Index [201], TW can be easily derived from temperature and humidity by means of thermodynamic equations [72] or, as in this report, by the empirical formula derived in [333]. The highest TW values recorded on Earth are close to 35 °C, which is considered the limit of survivability for a fit human being [321, 253]. This value would greatly reduce the possibility of evaporation at skin level to cool the body, since the skin (usually at 35 °C or below) must be cooler than the body core (around 37 °C) in order for metabolic heat to be conducted to it. In this report, three heat-stress-derived indices are considered (based on daily maximum values of TW): summer mean and maximum TW, and the number of summer days with TW above 22 °C. This threshold is chosen to account for intense heat stress, as it approximately corresponds to the observed summer 98th percentile of TW in Zurich and Geneva and the 92nd percentile in Lugano in the reference period.

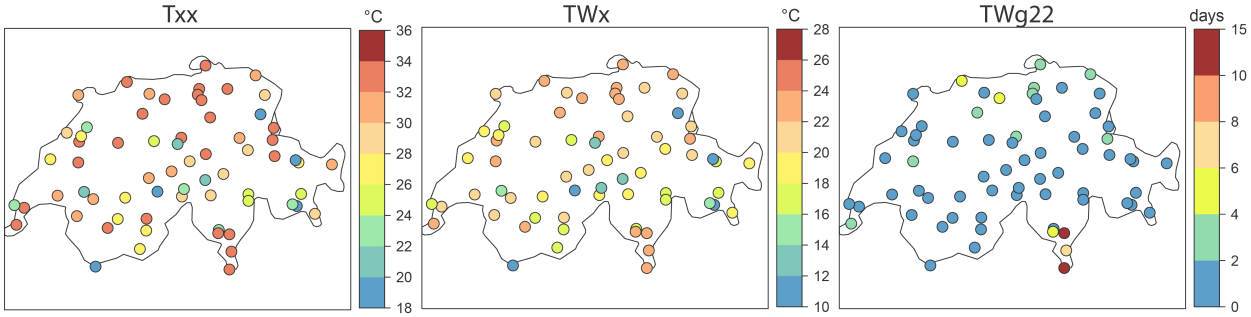

Figure 3.6. Observed values at 67 Swiss stations for the mean annual maximum temperature (TXx) and wet bulb temperature (TWx), both in °C, and the number of days with TW above 22 °C (TWg22) in summer (JJA) for the period 1981 - 2010.

Unlike the highest daily maximum temperature per year (*TXx*), which shows a markedly orographic spatial pattern, the highest daily heat stress (*TWx*) is between 18 °C and 24 °C at most of the non-mountainous stations (Figure 3.6). The threshold of 22 °C is, on average, only exceeded in a few locations, with the largest values in the low-lying stations in Ticino (7 days in Lugano and 12 in Magadino/Cadenazzo and Stabio). Unlike temperature, no gridded product is available for the heat stress indices at the moment, due to the lack of gridded specific humidity.

3.2.2. Precipitation

Although landlocked, Switzerland is still fairly close to the Atlantic Ocean and the Mediterranean Sea, which are important sources of humidity. Nevertheless, a transition from an oceanic (wet) climate in the western parts of the country to a more continental (dry) climate in the eastern parts can be observed within Switzerland. In addition, the complex Alpine topography leads to a large spatial variability in precipitation [125, 302, 173]. The annual precipitation sums vary by a factor of about five, from less than 600 mm in certain valleys in Valais in southwestern Switzerland to more than 3000 mm annually at some high-altitude regions of the central Swiss Alps. There are considerable differences in the annual cycles of precipitation sums in the different climatic regions, as illustrated by the histograms in Figure 3.7. The western Jura

mountains and western Plateau regions exhibit almost no annual cycle. Most other regions show a summer maximum, which is more pronounced in the eastern parts of the country. There, summer amounts of precipitation are larger by a factor of two or three compared to winter amounts. In the southern Alps, two maxima in spring and autumn are observed. All these characteristics are well explained by the dominant flow regimes (cf. Chapter 3.1) and convection activity in summer [173].

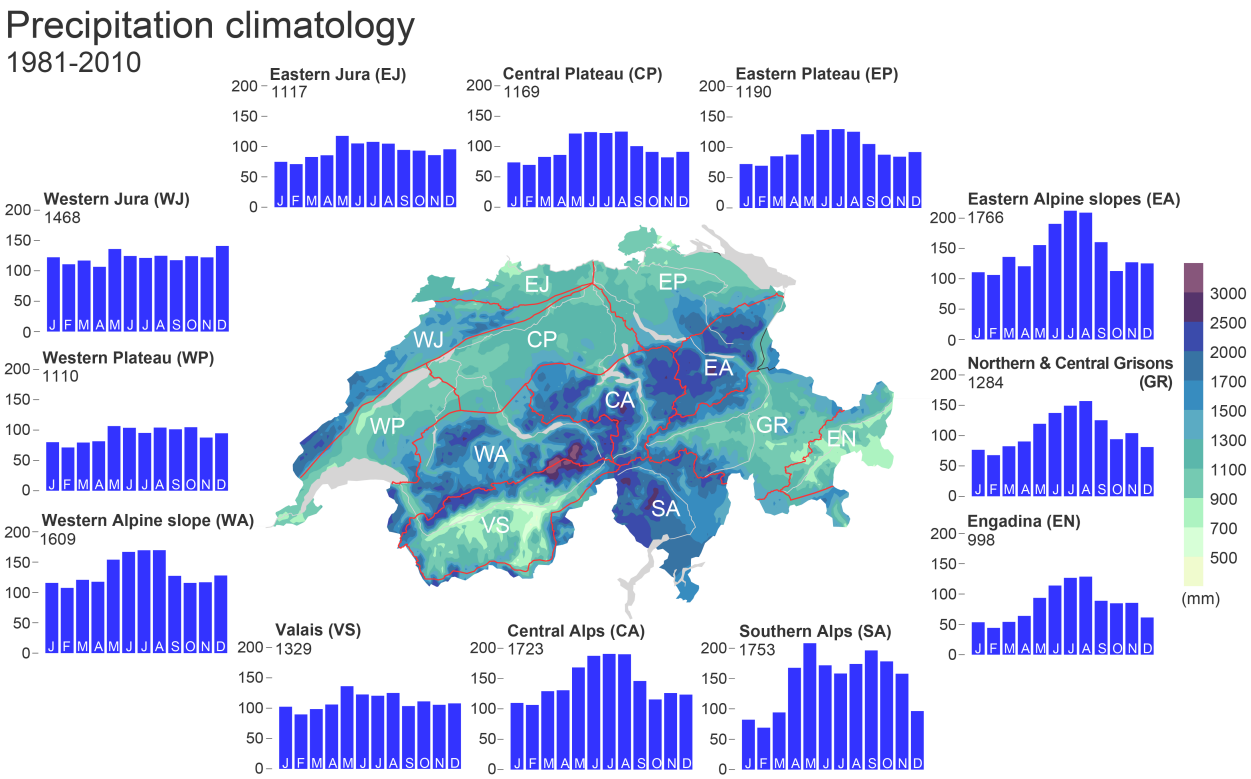

Figure 3.7. Gridded annual mean precipitation and monthly sums for the twelve Swiss climate regions after [227]. Regional annual means based on the gridded data are shown in the upper left corner of each barplot. Units: mm. Time period: 1981 - 2010. Data: MeteoSwiss gridded precipitation product RhiresM (see here for details).

To illustrate heavy and extreme precipitation in Switzerland, the 50-year return levels of 5-day, 1-day, 1-hour, and 10-minute precipitation are presented (cf. Figure 3.8; for technical details, see [129]). Note that the values shown on the maps have considerable uncertainty (often ±10 - 30 % or more for the 95 % confidence interval for a 1-day precipitation event for a 1-day precipitation event; cf. climate-extremes.ch for details). The most extreme precipitation events occur in Ticino on the southern side of the Alps, regardless of the duration of rainfall accumulation. In contrast, the inner-Alpine valley floors, especially the Rhone and Inn valleys, experience the most moderate heavy precipitation events within Switzerland. North of the Rhone and Rhine valleys, the spatial distribution of heavy precipitation varies with the duration of rainfall accumulation considered. For accumulations longer than a day, the northern Alpine rim and the Jura mountains experience heavier precipitation than the Plateau, whereas for sub-daily precipitation extremes, heavy precipitation generally does not seem to depend on altitude.

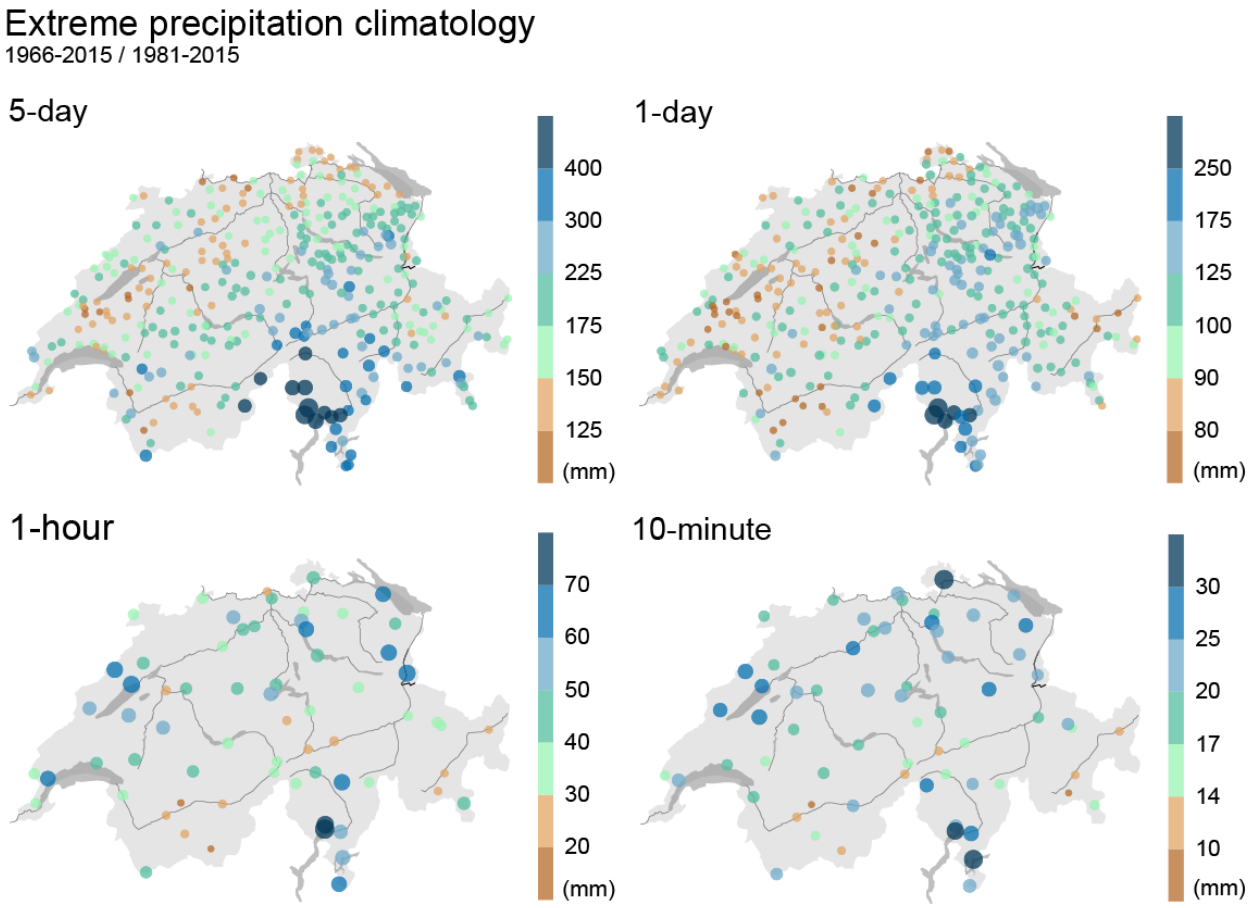

Figure 3.8. 50-year return values of 5-day (top left), 1-day (top right), 1-hour (bottom left), and 10-minute (bottom right) precipitation sums (in mm). Note that the color scale is different for each panel. The size of the circles is proportional to the return value and shows the same information as the color scale. The analysis period considered is 1966 - 2015 for the 1-day and 5-day sums and 1981 - 2015 for the 10-minute and 1-hour sums.

Another pertinent question is in which season the maxima occur and what processes lead to extreme events. For the 10-minute and 1-hour durations, the most extreme precipitation events in a year are generally associated with thunderstorms and, all over Switzerland, occur mostly in the summer months (source: MeteoSwiss). In contrast, the 1-day and 5-day durations exhibit more complex patterns (cf. [47] and MeteoSwiss). In summer, a high frequency of heavy 1-day and 5-day precipitation events along the northern Alpine rim and on the Plateau coincides with the tracks of thunderstorms, as revealed by the lightning climatology (see MeteoSwiss Website). In autumn, the high proportion of heavy precipitation events in Ticino reflects frequent situations in which a southerly flow of humid Mediterranean air impinges on the southern flank of the Alps. Interestingly, a considerable proportion of annual maxima occurs in winter in the Rhone valley and along the eastern flank of the Jura mountains.

> Much more information on Swiss precipitation extremes including a thorough assessment of their uncertainties can be found on the website climate-extremes.ch.

3.2.3. Snow

Due to the geographical location and the Alpine topography of Switzerland, a substantial fraction of precipitation falls as snow, and the water is stored for some time before it is released as meltwater. In CH2018, the analysis is restricted to basic features of snowfall and snow cover. Snow variables related to runoff, etc., are addressed in detail in the upcoming Hydro-CH2018 report.

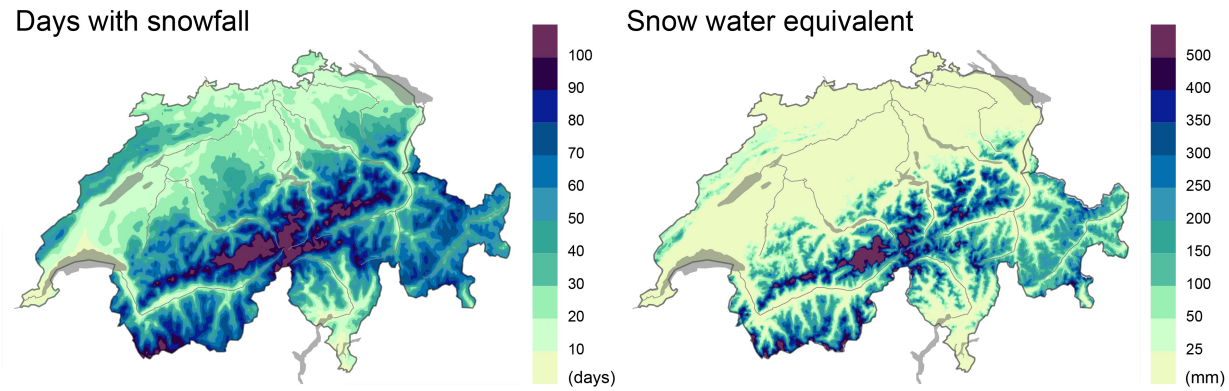

Figure 3.9. 1981 - 2010 snow climatology for the extended winter season (September - May). Left: Mean number of days with measurable snowfall based on [398] (days with new snow sum ≥ 1 cm). Right: Mean snow water equivalent (in mm, courtesy of T. Jonas, WSL).

The number of days with measurable snowfall strongly depends on altitude, with more days at higher altitudes (Figure 3.9). On the Swiss Plateau, roughly 10 to 30 days with snowfall are found in the September to May period. In the Alpine region, this number is higher, ranging between 30 and 120 days in most regions. In southern Switzerland, in the Rhone valley, and in the Lake Geneva region, the mean number of days with snowfall is less than 10. In terms of the mean snow water equivalent (SWE) [207], only a few millimeters of snow water are recorded on the Swiss Plateau and other low-altitude regions. In contrast, SWE values in the Alps are between 100 mm and 300 mm, with the highest values (up to 600 mm) in the Bernese and central Alps (Gotthard region).

3.2.4. Wind

Winds in Switzerland are forced by the large-scale flow patterns but are strongly altered by the country's complex topography and therefore exhibit considerable spatial variation (cf. Figure 3.10, left). Monthly mean wind data from MeteoSwiss has been homogenized for climate analysis (cf. [22]). The observed annual mean wind speed in the reference period (1981 - 2010) ranges between 0.93 m s^{-1} (Disentis) and 8.57 m s^{-1} (Chasseral). The highest mean wind speed is observed over the Jura mountain peaks, followed by the Alpine mountains with slightly lower values. The lowest mean wind speed is measured in the lowlands of the Swiss Plateau, Ticino, and some inner-Alpine valleys. Most stations in northern Switzerland and on mountain peaks experience the strongest mean winds during wintertime. In the southern Alps, Ticino, and many Alpine valleys, the maximum occurs in spring, in some inner-Alpine valleys, in summer (cf. also [135]).

The strong wind gusts (98th percentile of daily maximum wind speed) range between 13.5 m s^{-1} (Disentis) and 43.9 m s^{-1} (Jungfraujoch; cf. Figure 3.10, right). Note that the uncertainty of wind-gust measurements is considerable, especially for the high percentiles presented here. Furthermore, the exact location and exposition of the measurement station plays a considerable role, complicating the spatial interpretation of strong wind gusts. The strongest gusts generally occur on high Alpine mountain peaks (up to 44 m s^{-1}), on the Jura mountain crests (up to 36 m s^{-1}), and, albeit weaker gusts, in typical Föhn valleys (up to 29 m s^{-1}). The weakest gusts, at around 15 m s^{-1}, are observed in some inner-Alpine valleys and the lowlands of Ticino.

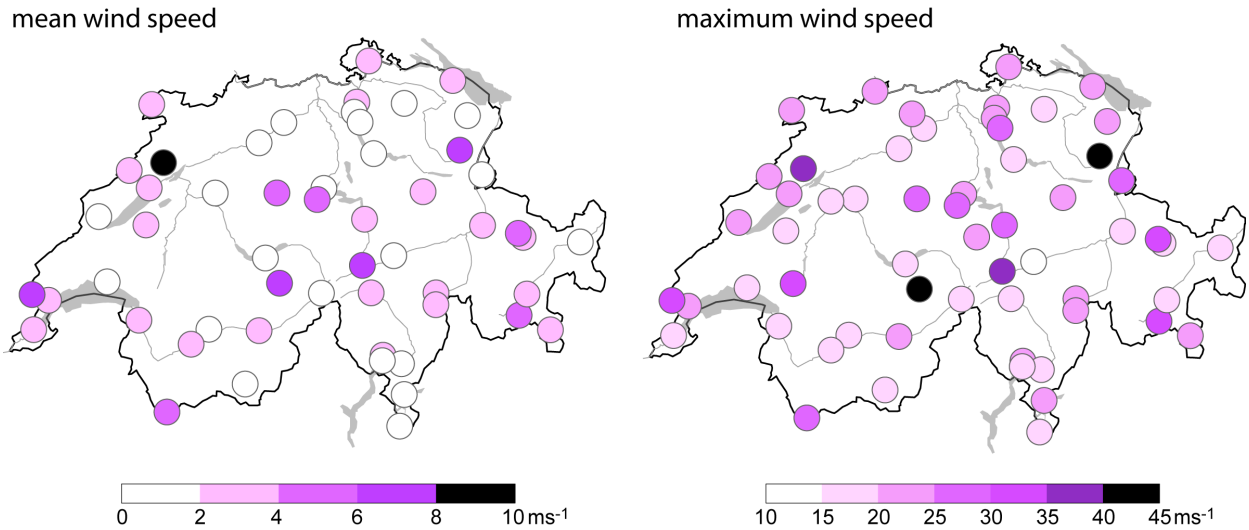

Figure 3.10. Mean wind speed (left) based on homogeneous data, and daily maximum wind speed (98th percentile, right) based on original data. Values are in m s^{-1} and are shown for the 1981 - 2010 reference period.

An analysis of the quality-checked strongest wind gusts since 1981 shows that the top-10 gusts in Switzerland are produced by a variety of wind types (cf. Figure 3.11). Winter storms are the most important causes, especially in northern Switzerland. In most regions, seven or more of the ten strongest events are caused by winter storms. In the northwestern parts of Switzerland, as many as all top-10 events are caused by winter storms. The main wind direction of winter storms is west or west-southwest. Wind gusts related to thunderstorms are in the top 10 at certain stations, mostly along the northern Alpine slopes, in the inner-Alpine valleys, and in southern Switzerland. North of the Alps and in inner-Alpine areas, the general wind direction of thunderstorm-related gusts is west, whereas in southern Switzerland, gusts show no preferred wind direction. In major Alpine valleys, most of the top-10 wind gusts are caused by the Föhn. Here, the wind direction is strongly affected by the orientation of the valley. In the Lake Geneva region, the Bise (from north-easterly directions) [366] is also be responsible for some top-10 wind gusts.

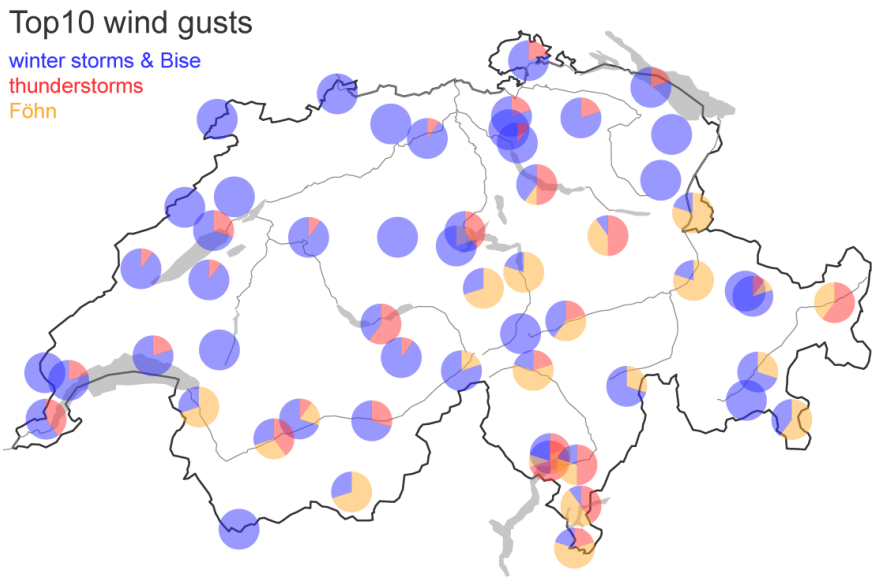

Figure 3.11. Classification of the top-10 wind-gust events at Swiss wind stations in the 1981 - 2017 period into "winter storms and Bise" (blue), "thunderstorms" (red), and "Föhn" (yellow).

For more information on the reference climate 1981 - 2010 (more parameters, gridded datasets, climate sheets at stations, climate indices, etc.) please visit the MeteoSwiss website meteoswiss.ch. For snow, also consult the website of the WSL Institute for Snow and Avalanche Research SLF (slf.ch).

3.3. Observed variability and recent change

3.3.1. Introduction

Possibly the most informative way to analyze the climate and especially its change over time is to examine the observed climate evolution. We restrict most of our analysis to the instrumental record covering the last 150 years, as this is the period in which the anthropogenic influence on the global climate became increasingly important. For summer temperatures and winter storms, reliable reconstructions based on documentary evidence and climate proxies going back to the year 1685 are used. For all other variables, the data source is high-quality observational climate data from the Swiss meteorological network, which was established in the year 1864. These long time frames, more than 150 years of measurements and more than 300 years for some reconstructions, are crucial for the correct identification of natural and anthropogenically forced changes in the climate system and the assessment of how strong the projected future changes will be. In the following sections, the variability and trends since the start of measurements/reconstructions are discussed. Extreme indices and their change signals are then presented. For a discussion of detection and attribution, the reader is referred to Chapter 7. For most analyses in this section, the period 1961 to 1990 is used as a reference period. This period, which should not be confused with the reference period 1981 to 2010 for climate projections, is still the valid standard normal period used by WMO and is often utilized for analyses related to climate change.

3.3.2. Temperature

Near-surface air temperatures in Switzerland exhibit large interannual to decadal variability. However, there is a pronounced long-term trend in the temperature data of almost 2.0 °C of warming between 1864 and 2016, or ~1.3 °C per 100 years using a linear trend estimate (Figure 3.12). The largest increases have occurred since the late 1980s. This trend has been discussed in many studies (e.g., [21, 274, 9, 55]). Warming in Switzerland amounts to more than twice the global warming rate of 0.9°C in the same time period (Figure 3.12). It is also greater than the warming of the Northern Hemisphere's land regions, which is about 1.3°C, and is on the upper end of the warming rates over the European domain based on global observational datasets like CRUTEM4, GHCNv3, GISSTEMP, and BEST [237, 145, 202, 280]. Nine of the ten warmest years since measurements began in 1864 have been recorded in the 21st century (cf. Figure 3.13). There has been no year with temperatures below the 1961 - 1990 mean in the last 30 years, and the annual temperature anomalies with respect to the period 1961 - 1990 are largely similar all across the country. Note that due to the strong recent trends, the 1981 - 2010 mean is about 0.8 °C higher than the 1961 - 1990 mean (cf. the different axis in Figure 3.12).

The long-term temperature trends show pronounced differences between regions and elevations on the seasonal scale ([21], and F. Isotta, 2018, personal communication). The Swiss Plateau warmed more than the Alpine regions in winter, but the opposite effect is found for summer. In spring and autumn, the warming is regionally more homogeneous. For most regions, the warming is somewhat stronger in autumn than in spring. It is not yet clear whether these differences are related to climate change, as has been proposed for some mountain regions in the world (e.g., [258]), or whether they are primarily caused by internal variability [55, 9]. On shorter timescales (a few decades), some signals of elevation-dependent temperature trends have been identified – for example, a strong cooling of high-altitude winters. These can be explained by natural variability producing unusual atmospheric flow conditions (cf. [10, 290] and Chapter 7). Slightly stronger temperature trends have also been identified near the snow line in spring, pointing to a small effect of the snow-albedo feedback (cf. [55, 299]).

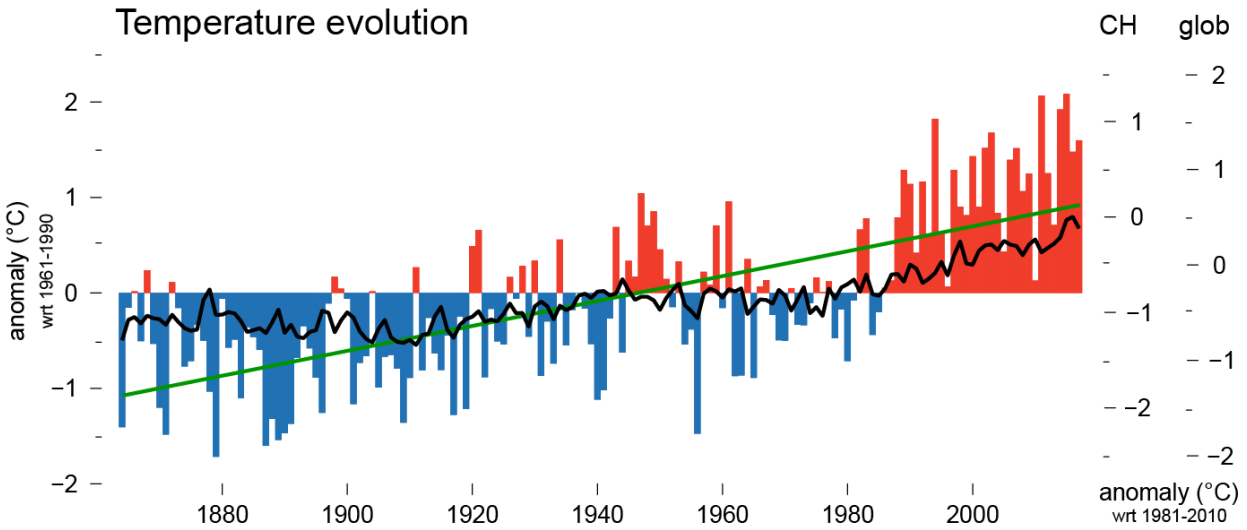

Figure 3.12. Evolution of Swiss and global annual mean temperatures, shown as deviation from the means for 1961 - 1990 (left axis) and 1981 - 2010 (right axes, left: Swiss series (CH) and right: global (glob)), the time frame used as reference period for the climate scenarios. The Swiss mean values (computed after [20]) are shown as bars with values above the 1961 - 1990 mean in red and values below the 1961 - 1990 mean in blue. The global values stem from the HadCRUT dataset (version 4.6.0.0, [237]) and are shown as a black line. The linear trend fit to the Swiss values is shown in green. Units: °C.

The observed Swiss temperature trend reflects an anthropogenic climate-change signal that is strongly modified by natural variability. The influence of natural variability is hard to quantify on regional and local levels (cf. Chapter 7 for more details). It is therefore important to note that the recent temperature increases can not be simply extrapolated into the future.

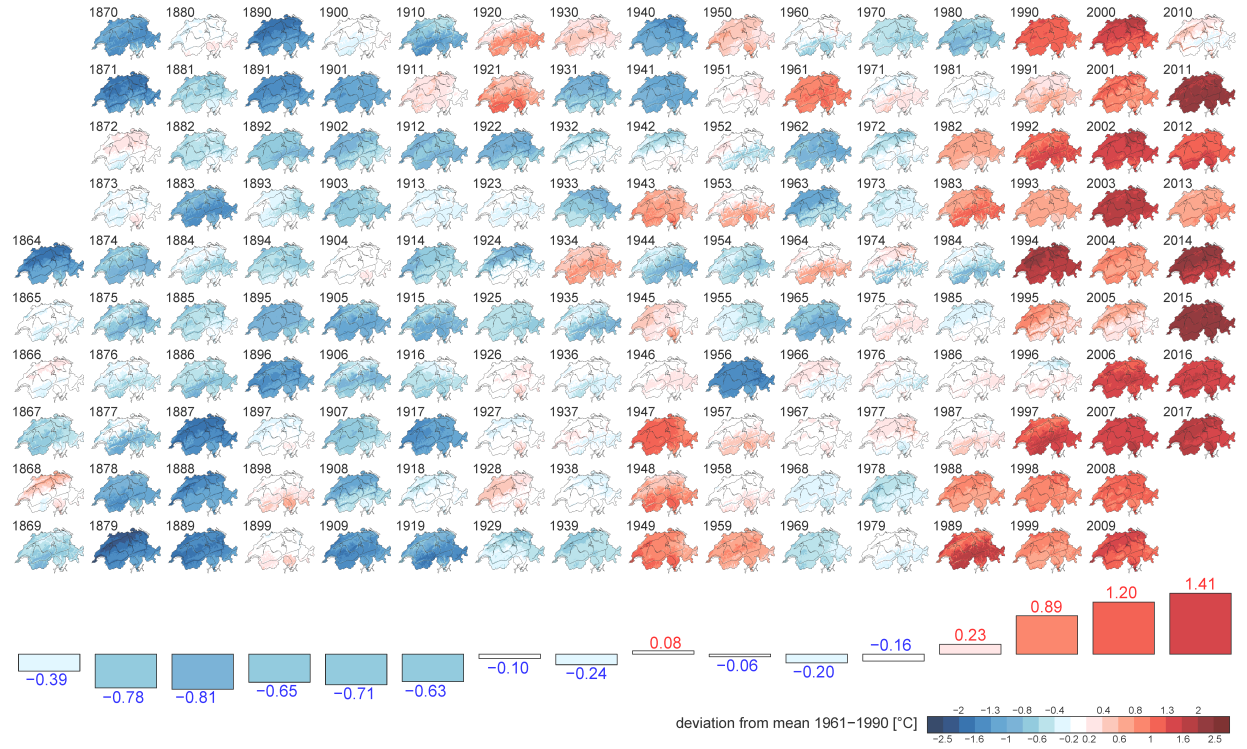

Figure 3.13. Maps of temperature deviation (in °C) from the mean for 1961 - 1990 for each year from 1864 until 2017 and decadal means for Switzerland (bars and numbers in the lower part). Years/decades above the mean are shown in red; years below the mean are shown in blue. Scale: -2.5 °C to 2.5 °C. Gridding method after [123], reconstruction by Isotta and Frei (in preparation).

There have also been significant changes in temperature extremes in the period 1864 - 2016. The coldest day, week, and two-week period warmed by +3.2 °C to 3.6 °C; this is considerably more than the increase for the warmest day, week, and two-week period, which (only) warmed by between +1.2 °C and 1.4 °C (cf. the slopes in the left and right panels of Figure 3.14). A possible reason for the smaller increases in the

temperature maxima is the declining sunshine duration and global radiation until about 1980 (see Chapter 3.3.6 for details). Not only the trend but also the variability in the cold extremes is considerably larger than that of the hot extremes. Very intense cold spells have been registered in 1929, 1956, 1963, 1985, and 1987. The trends in hot extremes for the period 1864 - 2016 reported here are somewhat lower than those in [298] for the the period 1901 - 2015. The frequency of hot periods has also changed significantly; notably, the rarer the event, the stronger the increase. [298] concluded that the number of days exceeding the 90th percentile of the 1961 - 1990 period increased by 94 % between 1901 and 2015 – and those exceeding the 95th and 99th percentile increased by 138 % and 212 %, respectively, in the same period – consistent with the findings of [77].

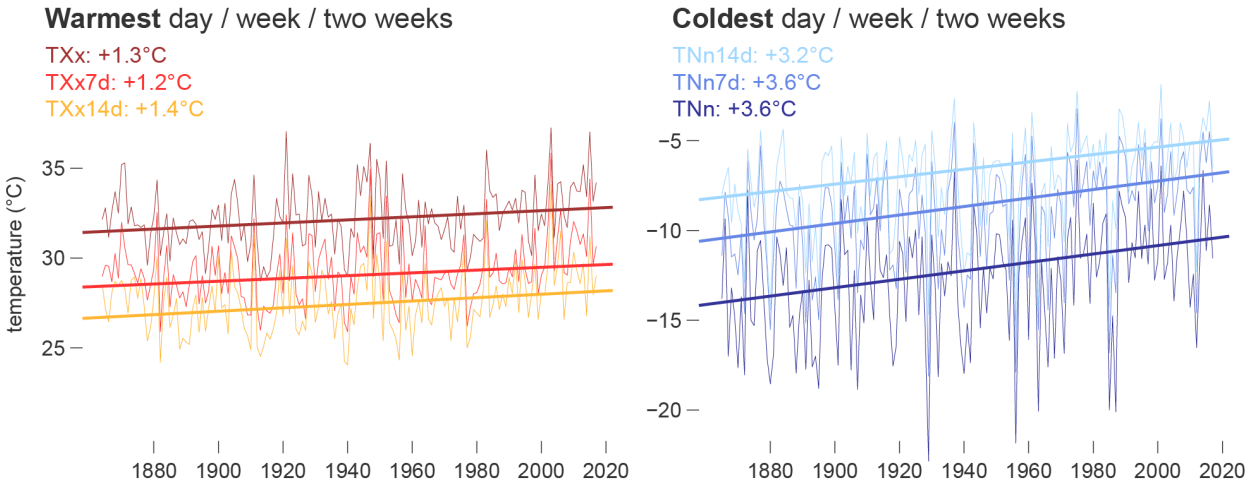

Figure 3.14. Time series of the warmest day (TXx, dark red), warmest week (TXx7d, red), and warmest 2-week period (TXx14d, orange) in the left panel and of the coldest day (TNn, dark blue), coldest week (TNn7, medium blue), and coldest 2-week period (TNn14d, light blue) in the right panel. Shown are the evolution of annual values (thin lines), a 20-year Gaussian smoother (bold line), the Theil-Sen linear trends (cf. [388], dashed lines), and the trend numbers (since 1864, in °C) on the Swiss Plateau (four-station mean for Zürich/Fluntern, Basel/Binningen, Bern/Liebefeld, and Genève-Cointrin).

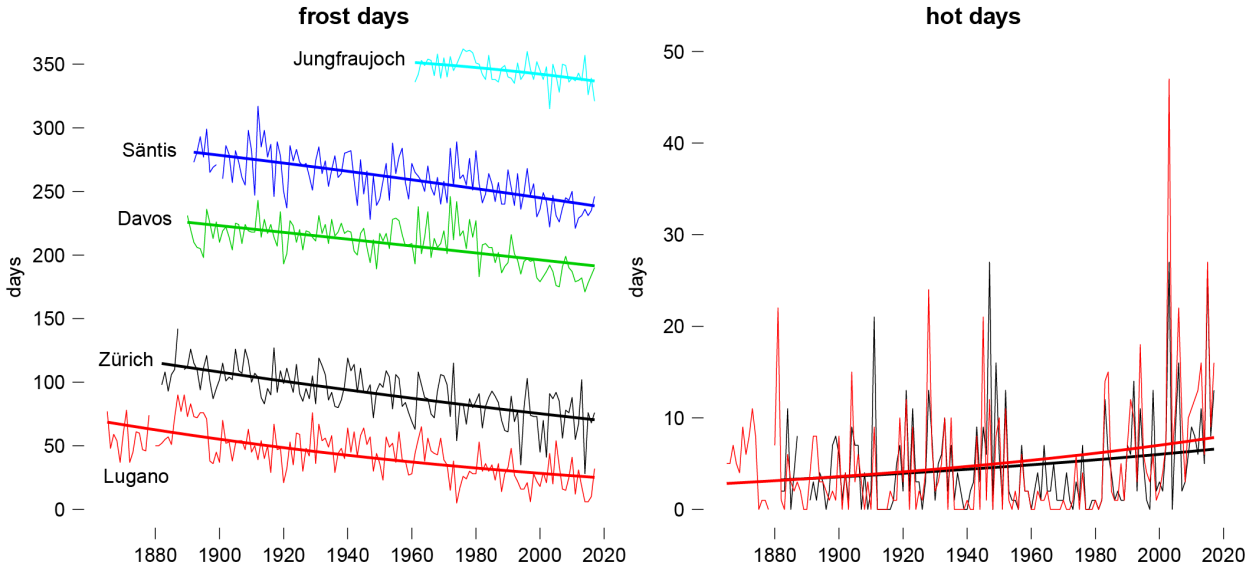

Figure 3.15. Evolution of the number of frost days (T_{min} < 0 °C, left) and the number of hot days (T_{max} ≥ 30 °C, right) for five Swiss stations (Lugano (red), Zürich (black), Davos (green), Säntis (dark blue), and Jungfraujoch (light blue)) since measurements began. The trend lines show fits using a logistic regression (e.g., [124]). Note that there have not yet been any hot days at the high-altitude stations of Davos, Säntis, and Jungfraujoch.

For practical purposes, threshold-based indices such as *frost days* (T_{min} < 0 °C) and *hot days* (T_{max} ≥ 30 °C) are often used (e.g., [392]). Figure 3.15 shows the changes in *frost days* (left) and *hot days* (right) since the measurements started in the 19th century. There is a distinct and highly significant decrease in the annual number of *frost days* at all altitude levels, with moderate changes of -5 % to -20 % since 1961 at high altitudes and the strongest declines, of the order of -60 %, at low altitudes (cf. also [231]). In contrast, strong

increases in the number of *hot days* are found. In the 1960s, only 1 to 3 *hot days* per year were observed in Zurich and Lugano, but these numbers have increased to about 10 days on average today.

Another intuitive temperature index is the altitude of the zero-degree line (degree Celsius), which can be defined using upper-air data or surface station data (cf. [36, 231]). This line has risen by 300 to 400 m or by roughly 150 to 200 m $°C^{-1}$ warming in the period from 1961 to today [231]. This change corresponds well to theoretical expectations based on an altitude shift in an atmosphere with a moist-adiabatic lapse rate of 0.5 °C to 0.67 °C per 100 m, which is very close to the current-day lapse rate in the Swiss Alps (cf. [200]). The long-term evolution of the zero-degree line in the winter season since 1864 shows a strong upward trend, but also substantial decadal variability (cf. Figure 3.16).

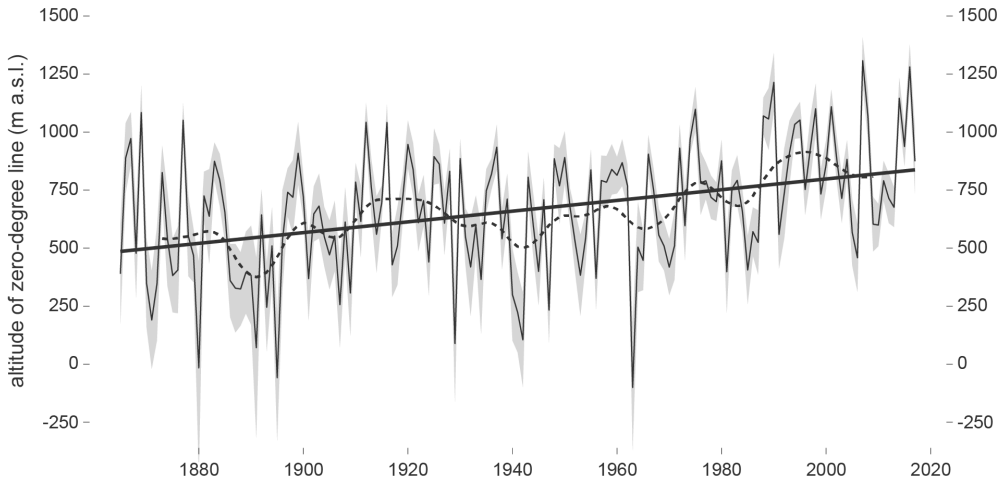

Figure 3.16. Evolution of the altitude of the winter (DJF) zero-degree line in Switzerland from 1864 to 2017 assessed from surface station temperatures (cf. [231] for methodological details). The black curve shows the best estimate; the grey range, the uncertainty of the value. The bold black line denotes the linear trend over the entire period, and the dotted line depicts the smoothed evolution using a 20-year Gaussian smoother.

Box 3.1: Summer temperature record since 1685

In addition to early instrumental measurements, which in Switzerland reach back to the mid-19 th century, summer (JJA) temperatures for the Swiss Plateau and the Alpine region have been reconstructed based on documentary evidence, tree rings, and other proxies [261, 53, 49]. The present assessment starts in 1685, in the middle of the Little Ice Age (LIA), a cold phase well described in the literature (e.g., [367]). For this period, various climate proxies agree relatively well, which is not always the case for earlier times.

The annual time series of summer mean (June to August) temperature from two different multi-proxy reconstructions using different techniques and focusing on different proxies (F, [121], and T, [345]) are shown together with the MeteoSwiss observational data (M, [20]) and the multi-station means of the Historical Instrumental climatological Surface Time series of the greater ALPine region (HISTALP, H, [48]) in Figure 3.17, a).

All series show a slight increase from the 17th to the mid-20th century, followed by a steep increase since the 1980s. Several particularly warm and cold summers stand out. The coldest summers occurred in the 1810s and include the “year without a summer” following the Tambora eruptions [268, 41]. The summers of 2003 and 2015 stand out as the warmest summers [306]. The summer 2018 not shown in Figure 3.17 ranked third and summer 2017 fourth. Since 1987, no individual summer has been colder than the 1961 - 1990 average. Summers were warmer around 1800 than in the decades before and after, particularly in the instrumental series (H). Possible instrumental biases (overheating of temperature screens, particularly in summer) have been discussed as a possible cause [120], but these have been taken into account in the dataset shown [48]. For a quantitative comparison to present climate reference periods (1961 - 1990 or 1981 - 2010), 30-year moving averages and confidence intervals are shown in Figure 3.17.

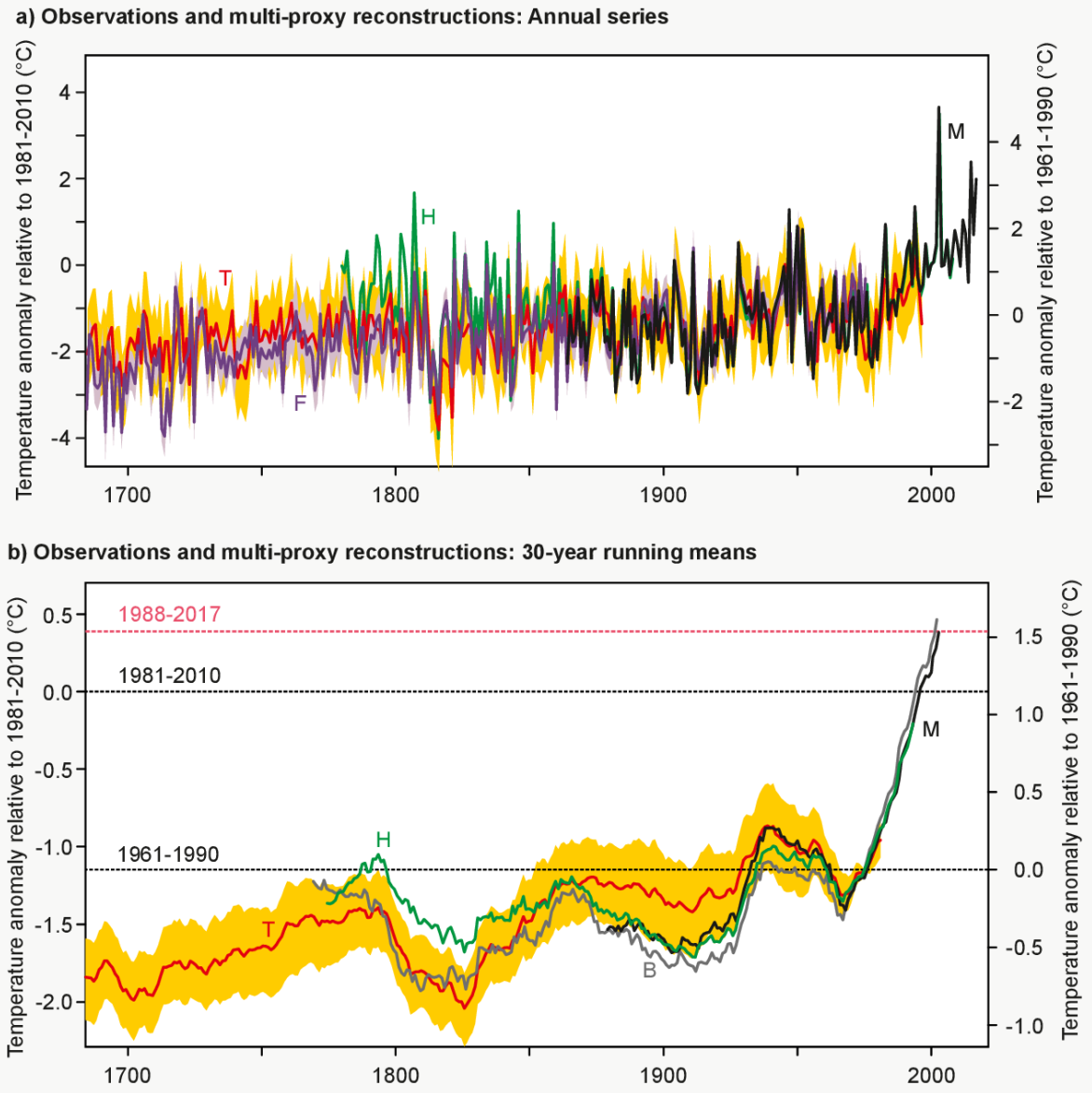

Figure 3.17. Time series of summer (JJA) temperature in the area of Switzerland/Alps. Top: Multi-proxy reconstructions by Trachsel et al. (2012) [345] (T, including 95 % confidence interval) and from a data assimilation by Franke et al. (2017) [121] (F, for the closest grid point up to 1975, ensemble mean, and range). Also shown are early instrumental measurements (H, HISTALP, [48] for the area 46° - 48°N/6° - 10°E) and the MeteoSwiss multi-station mean (M). Anomalies are indicated with respect to the 1981 - 2010 climatology (left axis) and the 1961 - 1990 climatology, which was used for calibration (the red dashed line indicates the most recent 30-year mean in M). Bottom: 30-year running means for the Trachsel et al. (2012) [345] reconstruction (T, red) with 95 % confidence interval (yellow), HISTALP (H, green), MeteoSwiss multi-station mean according to Begert and Frei (2018) [20] (M, black), and the series of Basel since 1755 (B, grey). The confidence interval for T accounts for the calibration of proxy data to an instrumental target; other uncertainties (e.g., associated with tree-ring measurements) are not accounted for.

The Trachsel et al. (2012) [345] summer temperatures are lower than the HISTALP temperatures between 1780 and 1830 (T, red in Figure 3.17, b), a period for which uncertainties in instrumental series are still high [48, 37, 178]. The coldest 30-year anomalies are found around 1700 during the so-called “Late Maunder Minimum”. During that time, summers were on average 0.8±0.3 °C colder than the 1961 - 1990 climatology or 2.2±0.3 °C colder than the most recent 30-year period (1987 - 2016). The figure further shows that the 1961 - 1990 average is unlikely to have ever been reached by any 30-year period during the LIA. Likewise, summer temperatures similar to those around 1980 (0.2 °C above 1961 - 1990) are unlikely to have been reached before the 1920s. The CH2018 reference period (1981 - 2010) is much warmer than the warmest period in the reconstruction. The recent 30-year period, 1988 - 2017, is 1.5 °C warmer than 1961 - 1990. In the longest Swiss instrumental series (from Basel), it is as much as 1.6 °C warmer than any 30-year period prior to 1961 - 1990.

3.3.3. Precipitation and drought

Due to the different precipitation regimes in Switzerland (cf. Figure 3.7), it is advisable to subdivide the trend analysis into different regions. Scherrer et al. (2016) [297] demonstrated that there are trend differences between the regions north and south of the main Alpine divide. Considerable and significant precipitation increases in the period from 1864 to the present day are only found in northern Switzerland (Swiss Plateau) for winter (~+20 % per 100 years, $p < 0.001$; Figure 3.18). In southern Switzerland, the trends are smaller and not significant (~+10 % per 100 years, p-value=0.20). In spring and autumn, no significant trends are found. In summer, trends are very close to zero (cf. [231]).

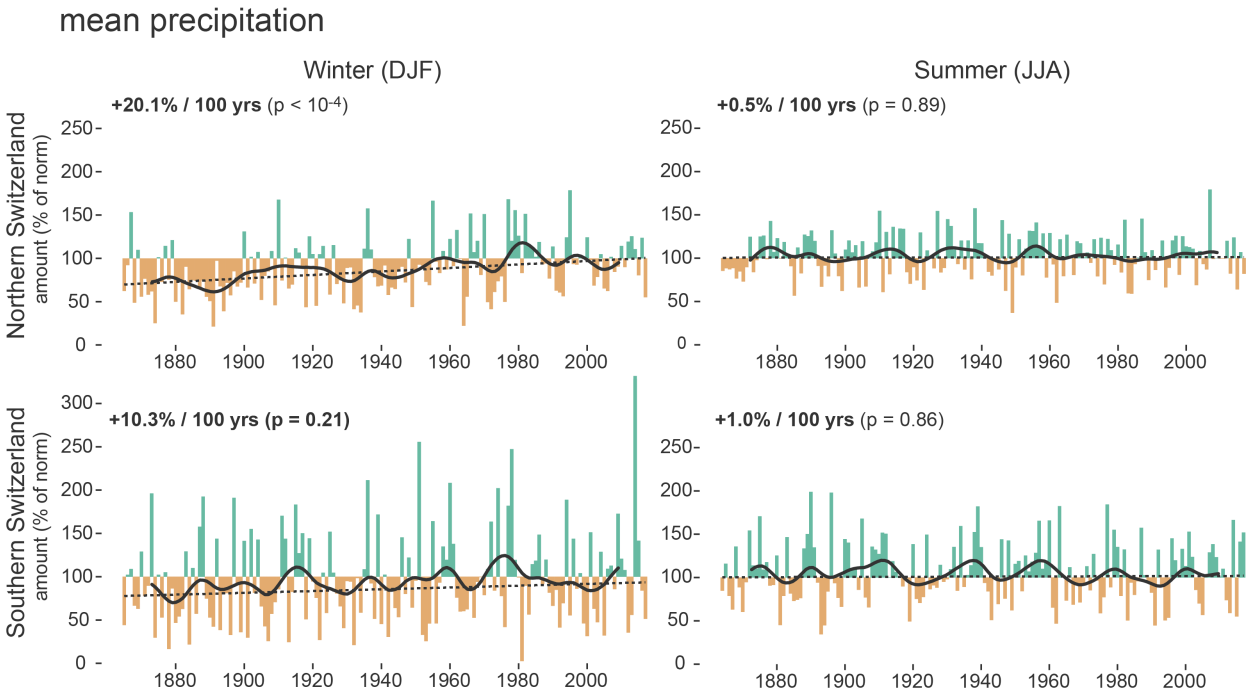

Figure 3.18. Precipitation from 1864 to 2017 for northern Switzerland (mean of Bern, Genève, Basel, and Zürich, top row) and southern Switzerland (Lugano, bottom row). Shown are seasonal amounts for winter (DJF, left) and summer (JJA, right) in percent of the 1961 - 1990 norm. Also shown are a 20-year Gaussian smoother (solid line) and the Theil-Sen linear trend fit (cf. [388], dashed line).

Reconstructions of summer precipitation for the Alps based on documentary data [261], early instrumental data [48], or multiple proxies [53] allow the identification of individual wet or dry years (or clusters of years), such as the dry summers around 1800 and those in the late 1940s. These data exhibit large uncertainties that are barely quantifiable, making trend estimates highly imprecise. It can additionally be noted that none of the existing reconstructions shows a clear long-term trend [39].

Extreme precipitation is rare by definition and subject to large interannual to decadal variability. It is therefore difficult to detect changes in extreme precipitation in the relatively short observational record (e.g., [64]). Consequently, the present analysis is restricted to heavy precipitation events that are rare in the sense that they occur on average only one to three days a year. Changes in both the intensity and the frequency of precipitation are of concern. Here, intensity trends are analyzed in terms of daily maximum precipitation sums (*Rx1d*; cf. [392]), and frequency trends in terms of the number of days exceeding the all-day 99th percentile (#R99e; cf. [298]). Intensity has increased by on average 12 % or 7.7 % per °C of warming since 1901 (Figure 3.19, a), a value close to that expected from the thermodynamic dependence of the water-holding capacity of air on temperature as described by the Clausius-Clapeyron scaling (e.g., [346]) and similar to the mean for a global dataset of several thousand stations [371]. Among the time series examined, 91 % show an increase, a fraction far greater than what would be expected by chance. The frequency of heavy precipitation events (1961 - 1990 period, 99th percentile; Figure 3.19, b) has increased by on average of 26.5 % since 1901. Over 92 % of the series show an increase, again a fraction far greater than what would be expected by chance.

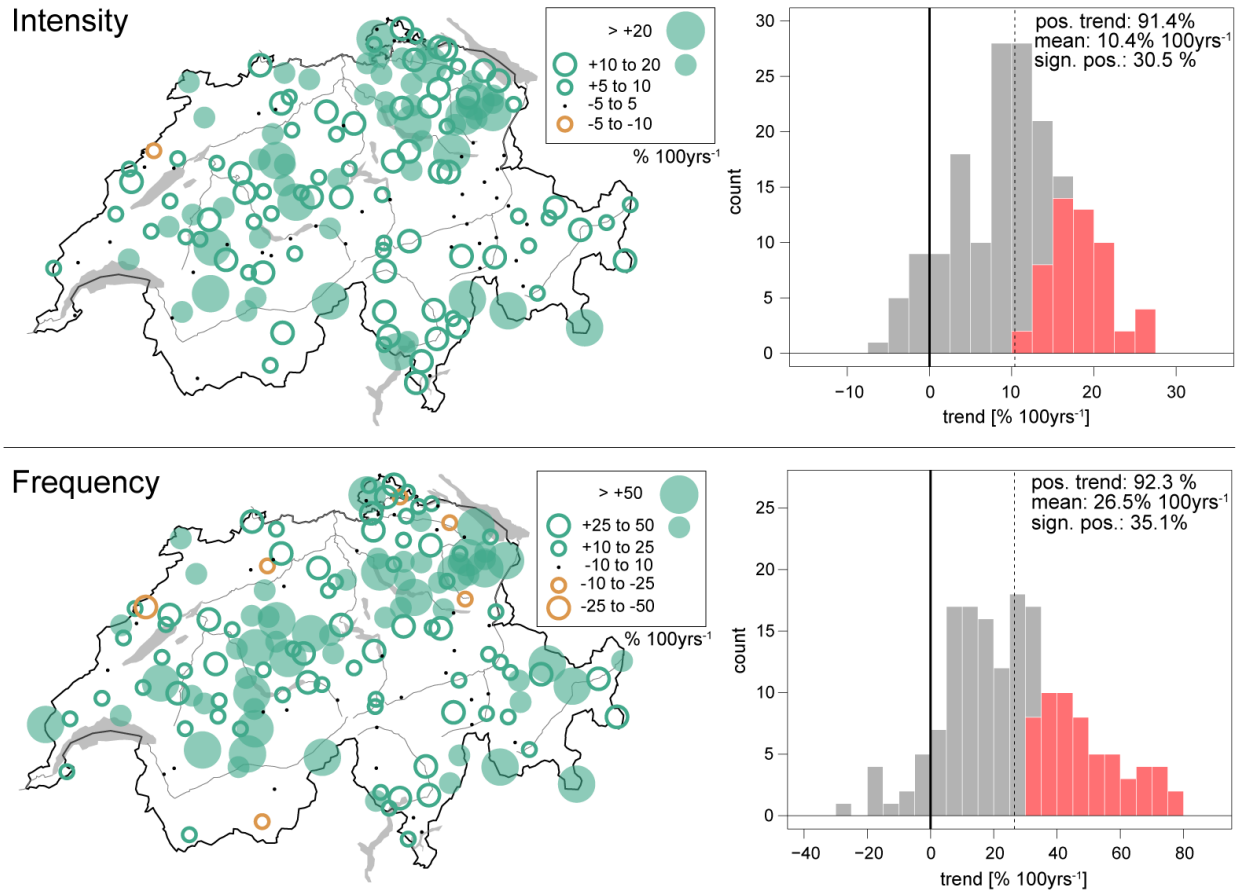

Figure 3.19. Observed 1901 - 2014 trends at ~170 Swiss precipitation stations of heavy precipitation, showing the annual daily maximum precipitation as the intensity measure (top), and of heavy precipitation frequency, showing the number of days exceeding the 1961 - 1990 all-day 99th percentile (bottom). Units are in percent per 100 years. Filled circles and red histogram bars indicate trends that are statistically significant at the 5 % level. Figure adapted from [298].

Drought can have a large impact on several sectors, including agriculture [381], water resources management, and energy production. The definition of drought is not straightforward and depends on the perspective of the stakeholders (cf. Chapter 6.7 for more information). Switzerland has experienced several meteorological and agricultural droughts since 1901 (i.e., 1911, 1945, 1947, 1949, 1952, 1959, 1962, 1976, 2003, 2011, 2015 and 2018; cf. [50, 309, 373, 251, 232]).

The evolution of agricultural droughts in the summer half year in Switzerland is described here using the Standardized Precipitation-Evapotranspiration Index (SPEI; cf. [357]). In addition to precipitation, the SPEI incorporates the effects of evapotranspiration on drought via a parametrization using air temperature. Here, evapotranspiration is parameterized by the potential evapotranspiration after [343]. This approach is known to have a tendency to overestimate changes in droughts, as the applied estimate of potential evaporation tends to be overestimated under high temperatures [320] and ignores several other important drivers of potential evaporation (radiation, wind, humidity), and because potential evaporation is a strong overestimate of actual evapotranspiration [233]. Several other drought indices exist, as analyzed in section Chapter 6.7. Nonetheless, in the absence of long measurement records of evapotranspiration or soil moisture [315], SPEI estimates can provide a first evaluation of the potential drying resulting both from precipitation deficits and from atmospheric demand for evapotranspiration.

There are no long-term SPEI trends, but the increasing evaporation due to positive temperature trends contributes to a negative but non-significant tendency. There is considerable decadal variability in the evolution of the SPEI on the Swiss Plateau (Figure 3.20), and most of the known drought years can be identified (cf. also [231, 232]). The strongest events in the summer half year according to the SPEI are 1865, 1911, 1947, 1949, 2003 and 2018 in northern Switzerland and 1870, 1893, 1921, 1962, and 2003 in southern Switzerland.

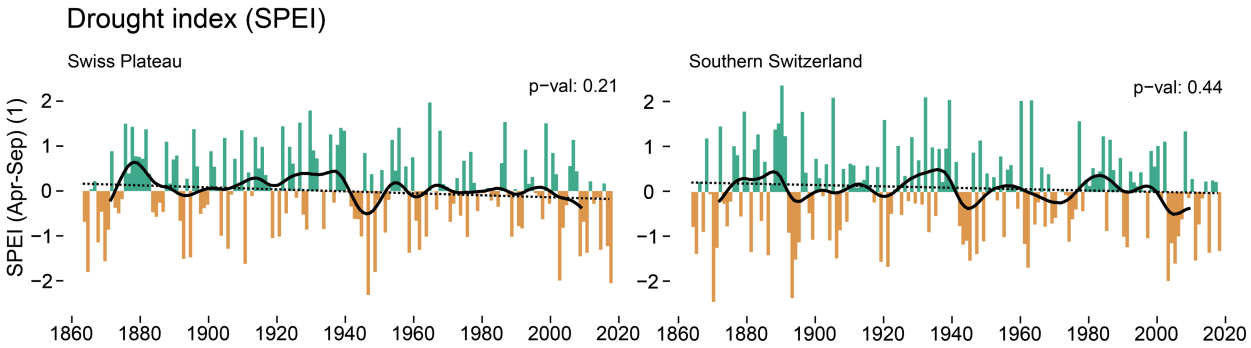

Figure 3.20. Standardized Precipitation-Evapotranspiration Index (SPEI) computed for the summer half year (April - September) 1864-2018 for the Swiss Plateau (left, average over the four stations of Zürich/Fluntern, Basel/Binningen, Bern/Liebefeld, and Genève-Cointrin) and for southern Switzerland (right, Lugano station). Also shown is a 20-year Gaussian smoother (thick lines) and the Theil-Sen linear trend fit (dashed line). The reference period for the SPEI computation is 1864 to 2018.

3.3.4. Snow and ice

In Switzerland, time series of new snow are available since the late 19th century for some stations. Snow height measurements, in contrast, are only more recently available but can be reconstructed with reasonable accuracy from new snow, temperature, and precipitation back to the late 19th century (cf. [299]. Long data series are required to put recent changes into context with natural variability and anthropogenic climate change [296, 294]. The snow series have been quality checked but not homogenized, and the influence of non-climatic artifacts cannot be entirely ruled out everywhere.

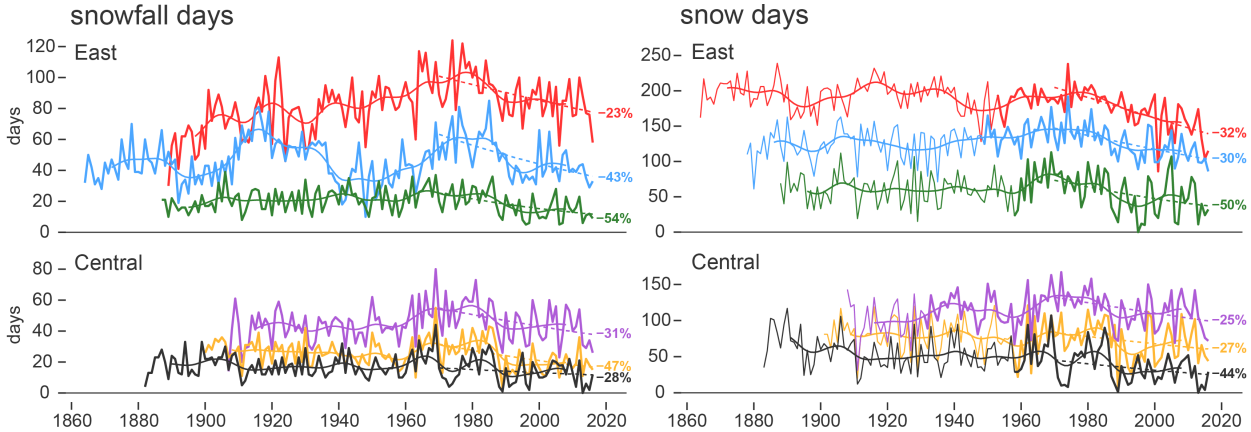

Figure 3.22. Number of days with snowfall (daily new snow sum ≥ 1 cm) per snow year (September 1 to August 31, left) and number of days with snowpack (daily snow height ≥ 1 cm) per snow year (right). The annual values are shown as a bold line; the thin line represents a 20-year Gaussian smoother. Top: Eastern Switzerland stations (Sils-Maria: red, Elm: blue, Chur: green). Bottom: Central Switzerland stations (Einsiedeln: purple, Meiringen: orange, Luzern: black). The dashed lines and numbers show the linear trends in the period 1970 - 2016.

For most stations, the lowest values and unprecedented negative trends in the snowfall and snow day records were observed in the late 1980s and 1990s (Figure 3.22; [299]). [217] and [316] demonstrate that after 1980, a shift-like decrease in the Swiss snow regime resulted in a reduction of the ratio of snowfall days to precipitation days by as much as 50 % below 800 m a.s.l. At higher elevations, around 2000 m a.s.l., the decrease is around 20 % since 1970. Very similar numbers are found for the number of snow days (cf. Figure 3.22, right panel) and by [189] for snow cover duration. This decrease is due to earlier snowmelt rather than to later snow onset. As demonstrated by time series of snow water equivalent, the large majority of sites in the Alps (even at the highest elevations) have seen a reduction in snow mass, which is more pronounced for spring than for winter (cf. [218]). Finally, it should be noted that not all snow variables show clear trends. The maximum new snow sums, for example, show no clear trends as yet (cf. [299]). Note also that the recent shift-like trends are often the result of the combined effect of forced trends and large natural variability (Chapter 7).

Changes in ice (glaciers, permafrost, lake ice) have not been assessed in this report. However, it has been shown in the literature that the Swiss and Alpine glacier area and volume have declined substantially ([391, 16, 143, 162, 112]). According to [391], the Alpine glaciers lost 35 % of their total area between 1850 and the 1970s, and almost 50 % by the year 2000. The Alpine glacier volume decreased by about 60% since the 1850s (e.g., [143]). [162] estimates the Alpine glacier volume losses in the period from 1900 to 2011 at about 96±13 km^3. In Switzerland alone, the glacier volume loss from 1980 to 2010 has been estimated to be 22.51±1.76 km^3 ([112]). The ice cover on Swiss lakes has also been significantly reduced since the mid-1980s (cf. [153]).

3.3.5. Wind

Wind speed and its potential changes are of interest for a wide range of applications (e.g., energy production, storms, warning systems). A decrease in wind speed was observed at most stations in Switzerland over the period 1981 - 2016 (cf. Figure 3.23). The absolute trends range from -0.21 m s^{-1} per 10 years (Chasseral) to less than 0.01 m s^{-1} per 10 years (Luzern). The most pronounced negative absolute trends were observed in the Jura mountains, parts of Valais, Grisons, and Ticino. The trends are significant ($p < 0.05$ using a Mann-Kendall trend test; cf. [388]) at most stations in Ticino, at some stations in Valais and Grison, at a few stations on the Swiss Plateau, on Chasseral, and in Interlaken. In order to judge whether these trends are extraordinary, it is important to put them into context with decadal variability.

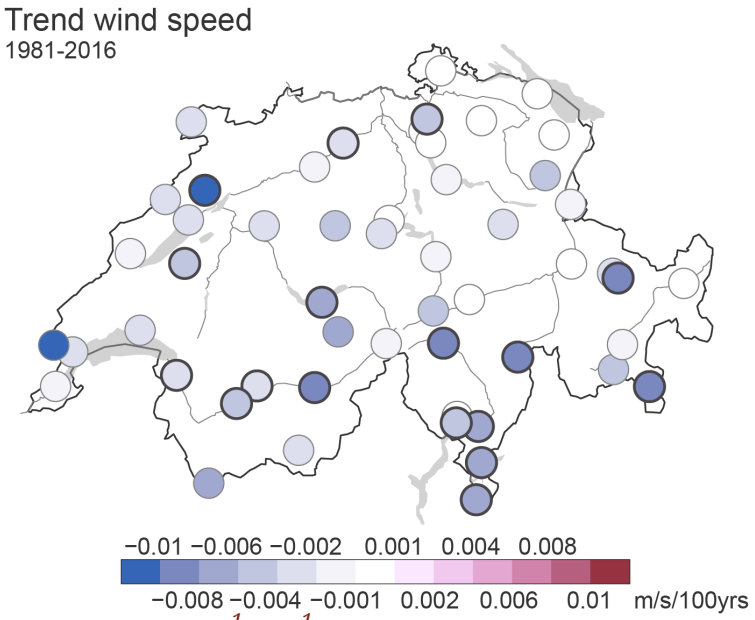

Figure 3.23. Linear trend of wind speed in m s^{-1} $year^{-1}$ for the period 1981 - 2016 based on homogeneous data. A thick black border on the symbol indicates that the trend is statistically significant at the 0.05 level (Mann-Kendall).

Switzerland has one long measurement series of wind speed, which is based on anemometer data from Zurich. From this record, evaluated hourly, homogenized daily maximum wind speed data have been derived [350]. Figure 3.24 shows the 96th percentile of daily maximum wind speed per winter half year (October - March) from 1851 to 2018. The year-to-year variations are in good agreement (though completely independent) with the 96th percentile of daily maximum wind speed from the Twentieth Century Reanalysis (20CR) Version 2c [67] for the grid point closest to Zurich. The Pearson (Spearman) correlation coefficient between measurements and 20CR is 0.56 (0.51). Both series display relatively pronounced multidecadal variability [42, 370]. The wind speeds in the 1981 - 2016 period are well within the band of the decadal variability since the mid-19th century.

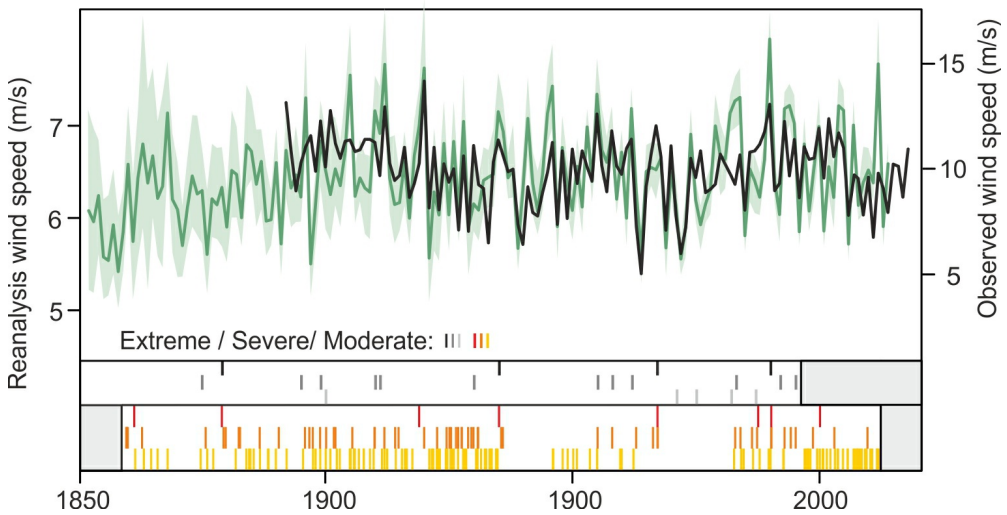

Figure 3.24. Winter windstorms in Switzerland 1851 - 2018. Top: 96th percentile of daily maximum wind speed in October to March in observations from Zurich (black) and the closest grid point in the Twentieth Century Reanalysis (green). The green shading shows the range of the 96th percentile in each of the 56 ensemble members of the reanalysis. Note that the scale is different, as maximum three-hourly wind speeds in the reanalysis are lower than maximum hourly wind speeds in the observations. Bottom: Occurrence of extreme, severe, and moderate windstorms in the catalogs of [38] in grayscale and [332] in color.

This strong decadal variability is also found in the independent damage-based storm catalog [332] and a windstorm catalog based on documentary data ([38], which excludes Föhn storms). Although the damage-based catalog might lack some of the moderate storms due to changes in the sources, very large events are unlikely to be missing. All sources agree that there have been decades or multi-decadal periods with more windstorms (e.g., ca. 1860 - 1875, 1890 - 1920, 1980 - 2000) and periods with fewer windstorms (e.g., 1940s to 1970s). The latter period is important, as it encompasses the “disaster gap” (cf. [262]), a period in which natural disasters were uncommon, and which had a strong influence on risk perception in Switzerland during a time of economic growth.

The long-term evolution of the Föhn, a typical topographic wind in the Swiss Alps, has been analyzed using the almost 150-year series of Altdorf [277]. The number of Föhn hours shows pronounced decadal variability but no clear long-term trend.

3.3.6. Sunshine, fog, and low stratus and small-scale phenomena

Sunshine duration is highly correlated (Spearman correlation r > 0.9 on the annual scale) with the amount of shortwave radiation reaching the ground [291, 351] and is therefore strongly influenced by cloudiness, but also to some degree by the transparency of the atmosphere to sunlight (air quality) in clear sky conditions. The long-term evolution of sunshine is of great interest also because it has a strong influence on temperature extremes. For the Swiss Plateau, four long series are available for analysis dating back to the late 19th century. Pronounced decadal variability and trends are found in the series from the Swiss Plateau and the southern Switzerland series of Lugano (cf. Figure 3.25). The values decrease from relatively high levels at the end of the 19th century and reach a distinct minimum around 1980. After 1980, the values increase strongly, rising back to the level of the maxima of the late 19th century in recent years. This is well in line with a widespread decrease in surface solar radiation between the 1950s and 1980s (global dimming) and a partial recovery more recently at many locations (brightening) [380, 378, 379]. The origins of these variations are mainly related to anthropogenic air-quality modifications through changes in aerosol emissions governed by economic developments and air pollution regulations. A preliminary analysis of observations of cloudiness shows that sunshine duration and cloudiness are highly anti-correlated (r ~-0.85 on the annual scale). To date, the contribution of changes in cloudiness and aerosols is not clear, although there are indications that changes in cloudiness alone cannot explain the strong increase in sunshine duration [291]. The high Alpine peak station Säntis shows no clear trend and no clear dimming or brightening effect since the late 1950s (Figure 3.25).

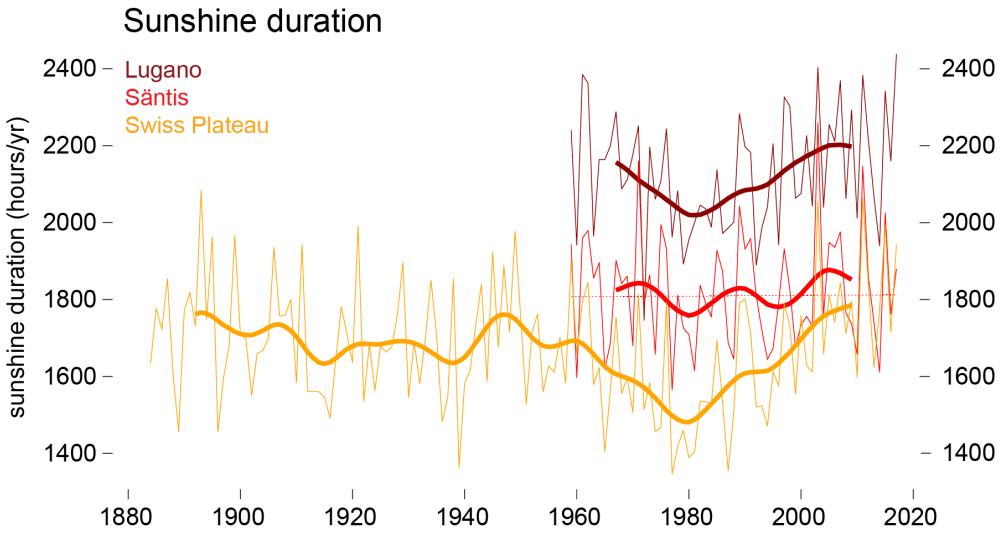

Figure 3.25. Observed evolution of averaged sunshine duration (in hours) since 1864 for the Swiss Plateau (mean of Zürich/Fluntern, Basel/Binningen, Bern/Liebefeld, and Genève-Cointrin, orange) and from 1959 onward for an Alpine peak (Säntis, red) and southern Switzerland (Lugano, brown). Shown are annual values (thin line), a 20-year Gaussian smoother (bold line), and a linear trend estimator for the Swiss Alpine peaks (dashed line).

Analyses of fog and low stratus series have found no clear long-term trend, but there is pronounced decadal variability with a maximum frequency in the late 1980s and early 1990s, followed by a minimum in the late 2000s [295]. A large fraction of the interannual variability and trends in fog and low stratus can be explained by the primarily natural variability of weather types [283]. It should be noted that for fog alone (using horizontal visibility), declining trends have been reported for the last few decades [361].

There is a large number of small-scale phenomena for which the available data series are too short or incomplete to make robust and reliable inferences on changes over the observational period. These include thunderstorms, hail, and tornadoes, but also pollen.